A&A 483, L29–L33 (2008)
DOI: 10.1051/0004-6361:200809761

Astronomy & Astrophysics

Letter to the Editor

First detection of hydroxyl in the atmosphere of Venus

G. Piccioni[1], P. Drossart[2], L. Zasova[3], A. Migliorini[1], J.-C. Gérard[4], F. P. Mills[5,6], A. Shakun[3], A. García Muñoz[5], N. Ignatiev[3], D. Grassi[7], V. Cottini[1], F. W. Taylor[8], S. Erard[2], and the VIRTIS-Venus Express Technical Team⋆

(Affiliations can be found after the references)

Received 11 March 2008 / Accepted 26 March 2008

ABSTRACT

Context. Airglow emissions, such as previously observed from NO and $O_2(a-X)$ (0–0) on Venus, provide insight into the chemical and dynamical processes that control the composition and energy balance in the upper atmospheres of planets. The OH airglow emission has been observed previously only in the Earth's atmosphere where it has been used to infer atomic oxygen abundances. The $O_2(a-X)$ (0–1) airglow emission also has only been observed in the Earth's atmosphere, and neither laboratory nor theoretical studies have reached a consensus on its transition probability.

Aims. We report measurements of night-side airglow emission in the atmosphere of Venus in the OH (2–0), OH (1–0), $O_2(a-X)$ (0–1), and $O_2(a-X)$ (0–0) bands. This is the first detection of the first three of these airglow emissions on another planet. These observations provide the most direct observational constraints to date on H, OH, and O_3, key species in the chemistry of Venus' upper atmosphere.

Methods. Airglow emission detected at wavelengths of 1.40–1.49 and 2.6–3.14 μm in limb observations by the Visible and Infrared Thermal Imaging Spectrometer (VIRTIS) on the Venus Express spacecraft is attributed to the OH (2–0) and (1–0) transitions, respectively, and compared to calculations from a photochemical model. Simultaneous limb observations of airglow emission in the $O_2(a-X)$ (0–0) and (0–1) bands at 1.27 and 1.58 μm, respectively, were used to derive the ratio of the transition probabilities for these bands.

Results. The integrated emission rates for the OH (2–0) and (1–0) bands were measured to be 100 ± 40 and 880 ± 90 kR respectively, both peaking at an altitude of 96 ± 2 km near midnight local time for the considered orbit. The measured ratio of the $O_2(a-X)$ (0–0) and (0–1) bands is 78 ± 8.

Conclusions. Photochemical model calculations suggest the observed OH emission is produced primarily via the Bates-Nicolet mechanism, as on the Earth. The observed ratio of the intensities of the $O_2(a-X)$ (0–0) and (0–1) bands implies the ratio of their transition probabilities is 63 ± 6.

Key words. planets and satellites: individual: Venus – infrared: solar system – techniques: spectroscopic – astrochemistry – molecular processes – radiation mechanisms: non-thermal

1. Introduction

The nightglow from the hydroxyl radical OH was discovered (Meinel 1950) in high-resolution spectra of the Earth's atmosphere in 1948, and OH was subsequently shown to play a key role in purging the atmosphere of pollutants harmful to the biosphere (Kley 1997). It is well-established theoretically that OH is important on Mars for stabilizing the carbon dioxide atmosphere against conversion on a large scale to carbon monoxide (Atreya & Gu 1994), although there has been no actual detection of hydroxyl there, probably due to the low predicted abundances. Hydroxyl produced from water vapor is also believed to play a vital role in sterilizing the environment at the Martian surface (Bullock et al. 1994), leading to the failure by the 1976 Viking missions to detect any organisms that may exist on Mars (Huguenin 1982). Although photochemical models have predicted OH nightglow emissions on other planets, the only reported attempt to observe them was carried out on the Martian atmosphere from the Mars-5 spacecraft (Krasnopolsky & Krysko 1976), but only an upper limit of 50 R was obtained. One Rayleigh, R, corresponds to the brightness of an extended source emitting 10^6 photons cm^{-2} s^{-1} in 4π sr. The ro-vibrational bands of the OH Meinel system has been, however, reported in comets (Tozzi et al. 1994), where water photodissociation is the most probable mechanism of excitation.

2. Observations

Following our studies of the O_2 nightglow emission (Drossart et al. 2007a; Gérard et al. 2008), we used the Visible and Infra-Red Thermal Imaging Spectrometer (VIRTIS) instrument (Piccioni et al. 2008; Drossart et al. 2007b) on the Venus Express spacecraft to look for fainter emissions on the night side of Venus. VIRTIS measures radiation intensity at wavelengths between 0.3 and 5 μm with a spectral sampling of about 10 nm in the IR. Observations with limb-viewing geometry are ideal for detecting very faint features, due to the long path along the line of sight. Under the assumption of a uniform distribution over the planetary globe, this amplifies the signal by more than a factor

⋆ The VIRTIS-Venus Express Technical Team: E. Ammannito[1], A. Barbis[2], R. Berlin[3], C. Bettanini[4], A. Boccaccini[1], G. Bonnello[5], M. Bouye[6], F. Capaccioni[7], A. Cardesin Moinelo[7], F. Carraro[8], G. Cherubini[2], M. Cosi[2], M. Dami[2], M. De Nino[9], D. Del Vento[7], M. Di Giampietro[2], A. Donati[2], O. Dupuis[6], S. Espinasse[8], A. Fabbri[2], A. Fave[6], I. Ficai Veltroni[2], G. Filacchione[7], K. Garceran[6], Y. Ghomchi[6], M. Giustini[2], B. Gondet[5], Y. Hello[6], F. Henry[6], S. Hofer[10], G. Huntzinger[6], J. Kachlicki[3], K. René[6], D. Kouach[6], A. Mazzoni[2], R. Melchiorri[6], G. Mondello[2], F. Monti[9], C. Neumann[10], F. Nuccilli[1], J. Parisot[6], C. Pasqui[2], S. Perferi[2], G. Peter[3], A. Piacentino[6], C. Pompei[2], J. M. Reess[6], J. P. Rivet[6], A. Romano[2], N. Russ[3], M. Santoni[2], A. Scarpelli[2], A. Semery[6], A. Soufflot[5], D. Stefanovitch[6], E. Suetta[2], F. Tarchi[2], N. Tonetti[2], F. Tosi[1] & B. Ulmer[3]. Affiliations: [1]INAF-IFSI Roma, [2]Galileo Avionica Florence, [3]DLR Berlin, [4]Università di Padova, [5]IAS Orsay, [6]LESIA, Obs. de Paris, [7]INAF-IASF Roma, [8]ASI Roma, [9]Techno System developments Naples, [10]Kayser Threde Muenchen.

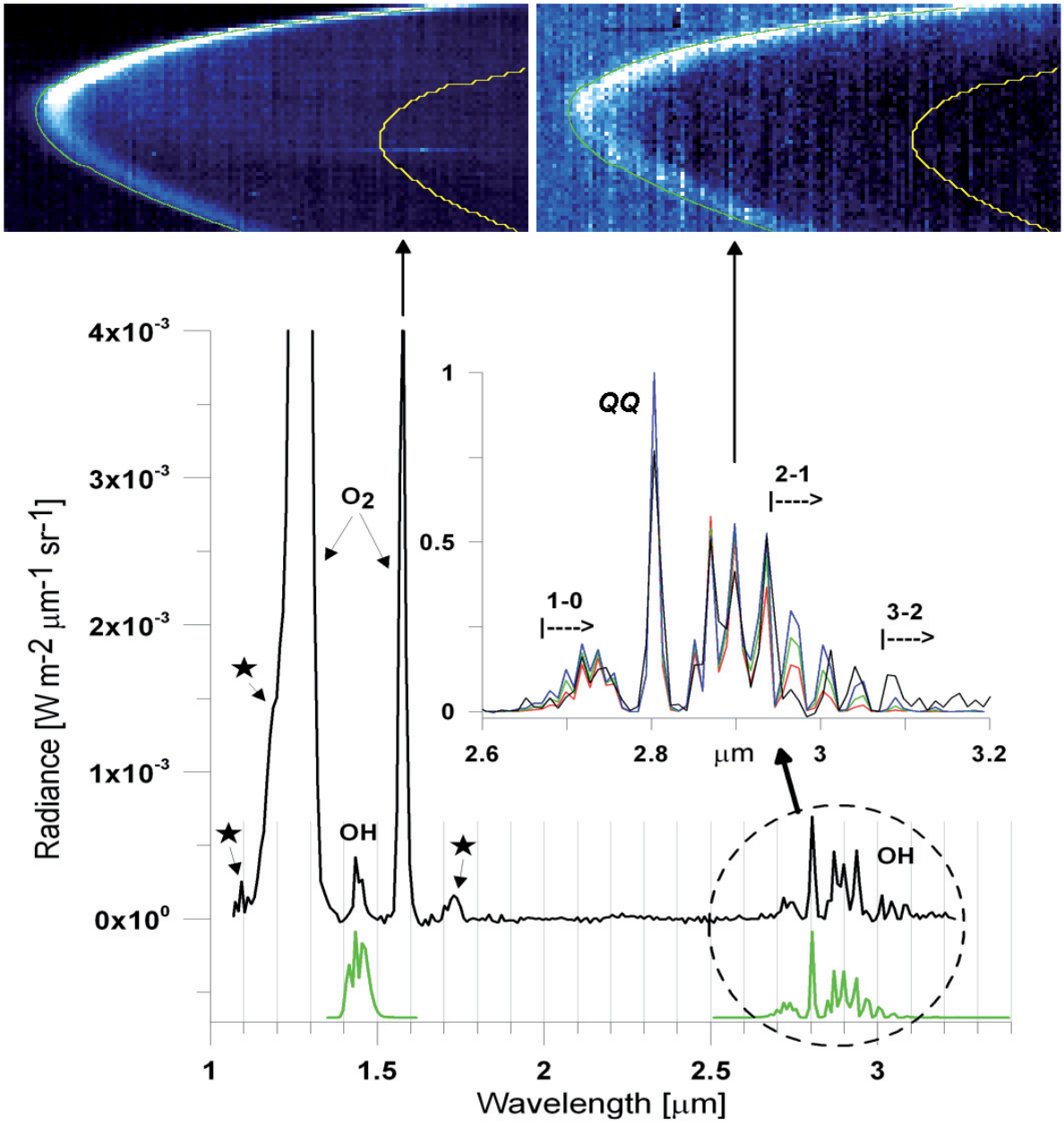

Fig. 1. Comparison of the observed radiance with OH synthetic spectra. The observed averaged radiance for orbit 317, latitude 15−25° N, local time 00:00 to 00:30 h, acquired 2007 March 4 is shown in black. The most prominent emission features at 1.27 and 1.58 μm are due to O_2. The other features are the OH fundamental bands at 1.44 μm (2−0) and 2.80 μm (1−0). The small features marked by asterisks at 1.1, 1.18, 1.74 μm are traces of the thermal emission from the lower atmosphere. In the insert, a fraction of the observed spectrum (black curve) is compared with synthetic spectra of OH for different rotational temperatures (200 K in red, 250 K in green, and 300 K in blue). The 250 K spectrum is also shown below the observed spectrum for the full range. At the top are the limb images for orbit 317 in the O_2 1.58 μm (*left*) and the OH 2.80 μm (*right*) emission bands (shown by arrows). Two altitudes above the surface are shown for comparison, at 0 km (yellow curve) and 100 km height (green curve). The elongated appearance is due to the use of a different linear scale for the vertical and horizontal directions.

of 50 compared to nadir measurements. It also makes a direct measurement of vertical distribution possible.

The observations reported here were obtained during orbit 317, 2007 March 4. The limb of Venus was scanned using the motion of the spacecraft while keeping the scanning mirror fixed. The slant distance ranged from 10 800 to 13 700 km, resulting in a geometrical vertical resolution of better than 3.5 km. The slit of the VIRTIS imager spans the entire altitude range of the atmosphere in each single frame, and a hundred frames are typically acquired in a few tens of minutes. To improve the signal-to-noise ratio, the spectra from the same altitude range were averaged over the latitude from 15 to 30 degrees north, and over the local time from 00:00 to 00:30 (Fig. 1). The most pronounced emissions are the $O_2(a - X)$ 1.27 and 1.58 μm bands, which come from the recombination of atomic oxygen produced mainly by the photolysis of CO_2 on the dayside, which is then transported by the circulation of the upper atmosphere to the night side.

The OH emission lines are unambiguously identified in the ranges 1.40−1.49 μm (2−0) and 2.6−3.14 μm (1−0) by comparison with synthetic spectra, shown in Fig. 1 for rotational temperatures of 200, 250, and 300 K. These use the line parameters from the HITRAN 2004 data base (Rothman et al. 2005) assuming rotational LTE, and are normalized to the peak at 2.80 μm.

The positions of all of the measured lines match the predictions to within 1.3 times the VIRTIS spectral width of 9.8 nm for the single band. Other OH vibrational bands with transitions $\Delta v = 1$ (2−1, 3−2 and 4−3) fall within the spectral range 2.7−3.3 μm. However, only the (2−1) band can be detected above the noise, consistent with the expectation that this will be the brightest emission if the excitation mechanism involves a non LTE (local thermodynamic equilibrium) process as commonly thought for the case of Earth (Lopez-Puertas & Taylor 2002). The instrumental spectral resolution limits the ability to distinguish the bands from the weaker transitions. Other small features are observed at 1.1, 1.18, 1.74 μm. These are traces of the thermal emission from the lower atmosphere in the windows between the CO_2 bands, which shows strongly in nadir spectra. Their presence in the limb spectrum means that they are scattered by haze that extends well above the main cloud decks to at least 90 km in altitude.

3. Results

The $O_2(a - X)$ 1.27 and 1.58 μm bands have a measured band-integrated intensity ratio of 78 ± 8, corresponding to 63 ± 6 in terms of the ratio of transition probabilities. The 1.58 μm observation is the first detection of this band in the spectrum of another planet. This is also the first simultaneous observation of the 1.27 and 1.58 μm emissions on any planet, including our own.

The measured emission rate of OH along the limb averaged from 90 to 100 km for the total integrated bands from 2.61 to 3.14 and 1.40 to 1.49 μm is found to be 880 ± 90 kR and 100 ± 40 kR, respectively, while the emission rate of the prominent Q11 branch at 2.80 μm of the (1−0) band has been measured to be 150 ± 14 kR. Their vertical emission rates are deduced to be 16 kR, 1.8 kR and 2.7 kR, respectively, assuming a factor of 55.4 to convert from the limb to the vertical direction and taking the observed vertical profile into account with a peak altitude at 96 ± 2 km (Fig. 2). For orbit 317, the emission from the OH (1−0) and (2−0) bands is 55 ± 5 and 480 ± 200 times weaker, respectively, than the 1.27 μm $O_2(a - X)$ (0−0) emission. In the ten orbits examined to date, these ratios vary from orbit to orbit by an amount of ±50%, but without a major change in the shape of the vertical profile, the peak altitude remaining constant within the vertical resolution of the measurement.

4. Discussion

The intensity distributions for the OH (1−0) and (2−0) Meinel bands identified in the Venus spectrum seem to be strongly spatially correlated with those of the $O_2(a - X)$ bands, and are diagnostic of the composition, chemistry, and dynamics of the upper atmosphere. Either reaction 1, the Bates-Nicolet mechanism, or reaction 2,

$$H + O_3 \rightarrow OH^* + O_2 \quad (1)$$

$$O + HO_2 \rightarrow OH^* + O_2 \quad (2)$$

could explain the observed intensities of the OH bands and the high degree of correlation in altitude with the $O_2(a - X)$ bands. On the Earth, vibrationally-excited OH near the mesopause is believed to be produced primarily via reaction (1) with the initial yield dominated by emission from states with vibrational quantum number $v = 6$−9, while lower vibrational states are populated via radiational and collisional quenching (Bates & Nicolet 1950; Dodd et al. 1994). No definitive requirement for production of vibrationally-excited OH on Earth via reaction (2) has been demonstrated (Dodd et al. 1994; Meriwether 1989), but it could make a significant contribution to the OH airglow on Venus where ozone abundances are smaller.

Profiles of OH airglow emission calculated from a model (Pernice et al. 2004) show reasonable agreement with the observations in Fig. 2, but with some deviations. If the OH emission is produced via reaction (1) and collisional quenching of OH proceeds via a single-quantum collisional cascade, a density product $[H]*[O_3]$ of $4–9 \times 10^{15}$ cm^{-6} and a net yield (García Muñoz et al. 2005) of about 6×10^{-2} at the altitude of the emission peak would produce a total emission rate of 500−700 kR along the line of sight, depending on the temperature, integrated over the (1−0) and (2−1) transitions. This value agrees well with the observed 880 kR. The (2−1) transition, if present, has been estimated from the model to contribute about 35% of the total. If the OH emission is produced via reaction (2) in the same hypothesis, a density product $[O]*[HO_2] = 1 \times 10^{15}$ cm^{-6} would produce an emission rate of 300−400 kR if all of the OH is produced in $v = 1$ and 500−600 kR if all of the OH is produced in $v = 2$ or higher. The effect of temperature on the production rate is more pronounced for reaction (1) than for reaction (2) through its effect on the ozone abundance.

The same calculation can be made for the (2−0) transition. In this case, an estimated net yield (García Muñoz et al. 2005) of about 8×10^{-3} for the OH produced via reaction (1) corresponds to an emission rate of 70−100 kR, very close to the observed 100 kR. reaction (2) could produce up to 80 kR, which is also consistent with the observations.

The simplest explanation is that reaction (1) is primarily responsible for both the observed (1−0) and (2−0) emissions, in which case the modeled contribution of O_3 photolysis to the day side $O_2(a - X)$ emission would be about 0.2−0.4 MR, incorporating the observed value of 0.3 MR (Connes et al. 1979). The observed variability of the intensity between orbits is probably related to the dependence on the physical conditions, especially temperature, of both the efficiency of the reaction and collisional quenching, although variability in the HO_2, H, O, and O_3 abundances can also be important. In particular, the layer at the altitude of the emission peak was recently reported to be quite hot and variable with time and latitude (Bertaux et al. 2007), enough to account for more than a factor of two variability in the O_3 abundance, which is consistent with the observed range of variability for the OH emission rate. The temperature estimated from the relative intensities of rotational lines in the (1−0) band is 250 ± 50 K, which is somewhat higher than the value of 185 ± 15 K deduced from the rotational distribution of the $O_2(a - X)$ emission (Connes et al. 1979). Similar sensitivity of OH and O_3 to temperature variations has been reported in model calculations for Mars (Zhu & Yee 2007).

These OH airglow observations provide direct information on the production rates for specific vibrational states of OH via the detected transitions. However, the implied total production rate for OH on the nightside is a factor of 5−6 larger than what has been calculated in global-average photochemical models (Pernice et al. 2004). The primary modelled losses for OH at 85−100 km are reactions (3) and (4), so by neglecting possible changes in [O] and [CO], global production of CO_2 via reaction (4) may be a factor of 2−3 greater than present models indicate:

$$O + OH \rightarrow H + O_2 \quad (3)$$

$$OH + CO \rightarrow H + CO_2. \quad (4)$$

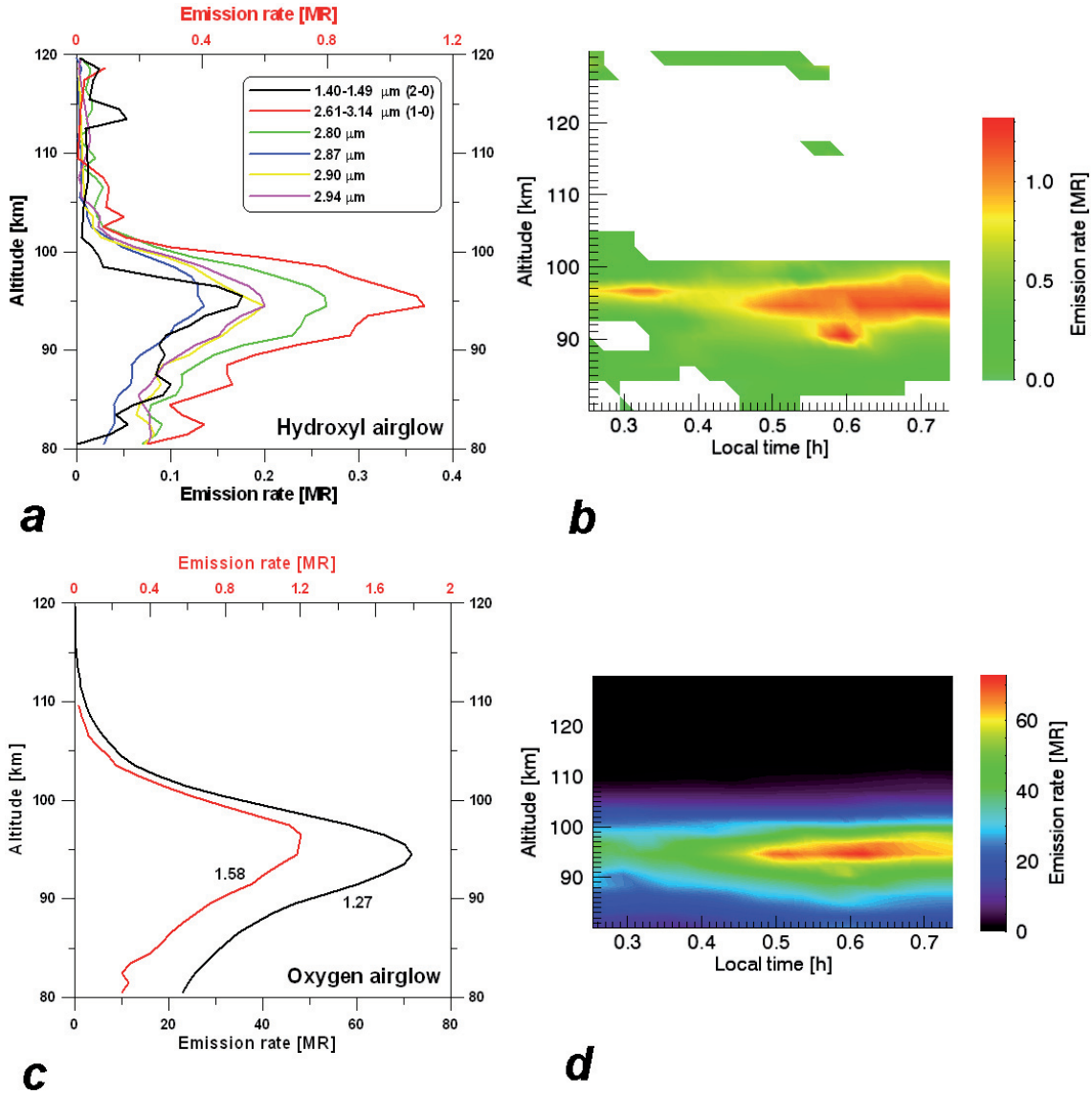

Fig. 2. Limb vertical profiles of the O_2 and OH nightglow emissions versus tangent altitude. Panel **a)**: vertical profiles of the OH emission at 2.80 μm (green), 2.87 μm (blue), 2.90 μm (yellow), 2.94 μm (magenta), plus all of these integrated from 2.61 to 3.14 μm (shown in red, only this one corresponding to the x axis on top in the same color, all the others refer to the bottom axis) and from 1.40 to 1.49 μm (black). Panel **b)**: the local distribution of the integrated bands (red curve of panel **a)** versus local time and tangent altitude of the closest point of the tangent limb to the planet. It can be seen that the distribution of the OH emission varies even within a single orbit. For comparison, the O_2 emission at 1.27 (black, bottom axis) and 1.58 μm (red, upper axis) is shown for the same orbit in panel **c)**, and its variability in panel **d)**. In all cases the instantaneous geometrical vertical resolution from the distance of 10 800 km to 13 700 is better than 3.5 km. In order to improve the signal to noise ratio, pixels are averaged over the latitude range 10−35° N and all profiles are smoothed with a step of 2 km in height.

reaction (4) is the dominant source of CO_2 on Mars, but chlorine catalytic chemistry most likely remains the dominant pathway for production of CO_2 on Venus.

5. Conclusions

The detection and measurement of OH on Venus provides new constraints on the dynamics of the upper atmosphere and on the chemistry and budgets of water vapor and carbon dioxide in the entire climate system of the planet. While the data are consistent with either of two mechanisms of production involving H, O_3, O, and HO_2, our current understanding of the photochemistry of terrestrial planet atmospheres favors the Bates-Nicolet mechanism as providing the main contribution to the OH airglow. The observed variability and the local distribution of the airglow in both limb and nadir geometries provide a way to map the distribution of these chemical species in the upper atmosphere of Venus. These may offer additional insights into chemical processes occurring on Earth and Mars.

Acknowledgements. We gratefully acknowledge the work of the entire Venus Express team that allowed these data to be obtained. We wish to thank A.S.I., C.N.E.S., and the other national space agencies that have supported this research.

References

Atreya, S. K., & Gu, Z. G. 1994, J. Geophys. Res., 99, 13133
Bates, D. R., & Nicolet, M. 1950, J. Geophys. Res., 55, 301
Bertaux, J.-L., Vandaele, A.-C., Korablev, O., et al. 2007, Nature, 450, 646
Bullock, M. A., Stoker, C. R., McKay, C. P., & Zent, A. P. 1994, Icarus, 107, 142

Connes, P., Connes, J., Noxon, F., Traub, W., & Carlton, N. 1979, ApJ., 233, L29
Dodd, J. A., Lipson, S. J., Lowell, J. R., et al. 1994, J. Geophys. Res., 99, 3559
Drossart, P., Piccioni, G., Gérard, J. C., et al. 2007a, Nature, 450, 641
Drossart, P., Piccioni, G., Adriani, A., et al. 2007b, Planet. Space Sci., 55, 1653
García Muñoz, A., McConnell, J. C., McDade, I. C., & Melo, S. M. L. 2005, Icarus, 176, 75
Gérard, J.-C., Saglam, A., Piccioni, G., et al. 2008, Geophys. Res. Lett., 35, L02207
Huguenin, R. L. 1982, J. Geophys. Res., 87, 10069
Meriwether, J. W. 1989, J. Geophys. Res., 94, 14629
Kley, D. 1997, Science, 276, 103
Krasnopolsky, V. A., & Krysko, A. A. 1976, Space Res., 16, 1005
Lopez-Puertas, M., & Taylor, F. W. 2002, Non-local Thermodynamic Equilibrium in Atmospheres (World Scientific)
Meinel, A. B. 1950, ApJ, 111, 555
Pernice, H., Garcia, P., Willner, H., et al. 2004, PNAS, 101, 14007
Piccioni, G., et al. 2008, VIRTIS: the Visible and Infrared Thermal Imaging Spectrometer, Tech. Rep. ESA-SP-1295 (ESA, Noordwijk, The Netherlands), in press
Rothman, L. S., Jacquemart, D., Barbe, A., et al. 2005, JQSRT, 96, 139
Tozzi, G. P., Feldman, P. D., & Weaver, H. A. 1994, A&A, 285, L9
Zhu, X., & Yee, J.-H. 2007, Icarus, 189, 136

[1] INAF – IASF (Istituto di Astrofisica Spaziale e Fisica Cosmica), via del fosso del Cavaliere 100, 00133 Rome, Italy
e-mail: Giuseppe.piccioni@iasf-roma.inaf.it
[2] LESIA, Observatoire de Paris, CNRS, UPMC, Université Paris-Diderot, 5 place Jules Janssen, 92195 Meudon, France
[3] Space Research Institute of Russian Academy of Sciences (IKI), Profsojuznaja 84/32, 117997 Moscow, Russia
[4] LPAP, Université de Liège, 17 allée du 6 août, B5c, 4000 Liège, Belgium
[5] Research School of Physical Sciences and Engineering, Australian National University, Canberra, ACT 0200, Australia
[6] The Fenner School of Environment and Society, Australian National University, Canberra, ACT 0200, Australia
[7] INAF-IFSI (Istituto di Fisica dello Spazio Interplanetario), via del fosso del cavaliere 100, 00133 Rome, Italy
[8] Atmospheric, Oceanic and Planetary Physics, Oxford University, Oxford OX1 3PU, UK